Construction and Building Materials 293 (2021) 123289

Contents lists available at ScienceDirect

Construction and Building Materials

journal homepage: www.elsevier.com/locate/conbuildmat

One-pot synthesis of monolithic silica-cellulose aerogel applying a sustainable sodium silicate precursor

Y.X. Chen [a,b], S. Sepahvand [a,c], F. Gauvin [a], K. Schollbach [a], H.J.H Brouwers [a,b], Qingliang Yu [a,d,*]

[a] Department of the Built Environment, Eindhoven University of Technology, P.O. Box 513, 5600 MB Eindhoven, The Netherlands
[b] State Key Laboratory of Silicate Materials for Architectures, Wuhan University of Technology, Wuhan 430070, PR China
[c] Department of Wood and Paper Science and Technology, Natural Resources Faculty, University of Tehran, Iran
[d] School of Civil Engineering, Wuhan University, Wuhan 430072, PR China

HIGHLIGHTS

- Sodium silicate produced from olivine silica was used as green silica precursor.
- Composite aerogel is synthesized by adding cellulose fibers using the sol-gel process.
- Specific surface area of prepared silica-cellulose aerogel can reach 958 m^2/g.
- Improved mechanical property and thermal stability were oberved for silica-cellulose aerogel.
- The hydrophilic silica-cellulose aerogel is hydrophobized, reaching contact angle of 140°.

GRAPHICAL ABSTRACT

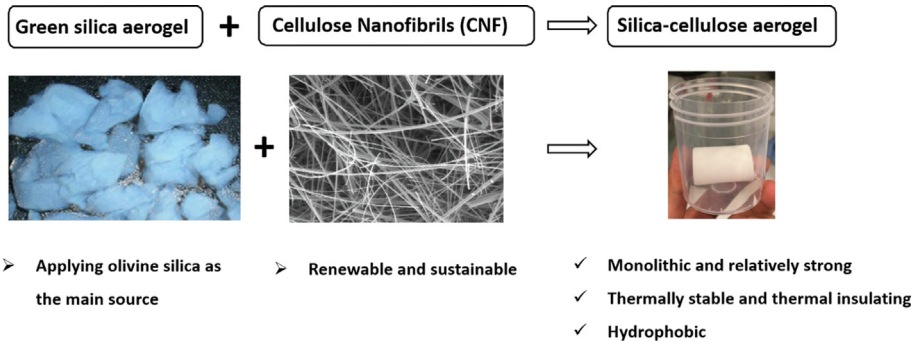

ARTICLE INFO

Article history:
Received 17 December 2020
Received in revised form 18 February 2021
Accepted 6 April 2021

Keywords:
Cellulose nanofibrils
Silica
Aerogel
Thermal conductivity
Sustainability

ABSTRACT

Cellulose aerogel is an advanced thermal insulating biomaterial. However, the application of cellulose aerogel in thermal insulation still faces critical problems, for instance, the relatively low strength and large pore size without Knudsen effect. In this study, a silica areogel made from olivine silica rather than traditional tetraethoxysilane or water glass is employed to synthesize silica-cellulose composite aerogel applying a facile one-pot synthesis method. The silica aerogel nanoparticles are formed inside the cellulose nanofibrils by using sol-gel method and freeze-drying. The developed silica-cellulose composite aerogel has an obviosuly lowered thermal conductivity and is significantly stronger compared to plain cellulose aerogel. The microstructure of silica-cellulose aerogel was characterized by SEM, TGA, FTIR and N_2 physisorption tests. The developed silica-cellulose aerogel had a bulk density of 0.055 ~ 0.06 g/cm^3, compressive strength of 95.4 kPa, surface area of 900 m^2/g and thermal conductivity of 0.023 W/(m·K). The thermal stability of the composite aerogel was also improved and showed the higher cellulose decomposition temperature. Furthermore, the composite aerogel is modified by trimethylchlorosilane making it hydrophobic, reaching a water contact angle of ~ 140°, enhancing its volumetric and thermo-phycial stability when applied in a humid environment. In conclusion,

Abbreviations: ϕ, Porosity; *Ps*, Skeleton density of aerogel; ρ_b, Bulk density of aerogel; λ, Thermal conductivity; *E*, Young's modulus; σ^*, Fracture stress; S^*, Strain; WG, Water Glass; SA, Silica Aerogel; SS, Silica Sol; NCA, Nano-cellulose Aerogel; SCA, Silica-Cellulose Aerogel; CNF, Cellullose Nano-Fibrils; SEM, Scanning Electron Microscopy; TEM, Transmission Electron Microscopy; TG, Thermogravimetry analysis; BET, Brunauer–Emmett–Teller theory; BJH, Barrett-Joyner-Halenda theory; TMCS, Trimethylchlorosilane; SSA, Specific Surface Area; FTIR, Fourier-Transform Infrared Spectroscopy; DT, Decomposition Temperature.

* Corresponding author.
E-mail address: Q.yu@bwk.tue.nl (Q. Yu).

https://doi.org/10.1016/j.conbuildmat.2021.123289

the resulting green silica-cellulose aerogel is a promising candidate for utilization as a high performance insulation material.

1. Introduction

Aerogel was first invented in 1931 by extracting the solvent in a silica gel without collapsing the silica gel structure [1]. Aerogel shows unique properties compared to other lightweight materials, such as polycarbonate, carbon fiber reinforced plastic or aluminum [2]. Thanks to the high porosity ($\phi > 95\%$) and low thermal conductivity, aerogels are excellent materials for thermal insulation, catalytic support and chemical absorbers [3-8]. Nowadays, with the increasing demand on green chemistry, aerogel made from nanocellulose have gained much focus due to its wide availability and renewability. Cellulose nanofibers are lightweight, mechanically strong nano/microfibers produced from plant-based materials [9]. Normally, it is applied in the textile industry and in bio/polymer composite fields as well. Cellulose mainly consists of repeating glucose molecules units attached to each other. Compared to other polymer fibers from petrochemical resources, naturally occurred cellulose fibers are acknowledged as a sustainable and green alternatives with high aspect ratio and specific surface area [10].

However, although cellulose aerogel has a very high porosity that beyond 97% and good formability, the thermal insulation property still cannot comparable to conventional silica aerogel. This is due to the much bigger pore size between cellulose fibers (around tens of micrometers) and hence the Knudsen effect cannot play a major role in the thermal conduction. Moreover, cellulose aerogel has a quite low strength compared to other aerogels, for instance, polymer aerogels like PU (Polyurethane) and PI (Polyimide) aerogels, which limits the application of its use in real world. Therefore, finding a suitable method to decrease the thermal conductivity and increase the strength simultaneously is still in demand.

Silica aerogel, on the other hand, is a conventional aerogel mainly used for thermal insulation, for instance, building energy saving, subsea pipeline heat conservation and interior insulation coatings [11-14]. However, silica aerogel is more fragile than other aerogel materials, such as cellulose aerogel. Therefore, most commercial silica aerogels are in the form of small granules or powder, making it difficult to apply them in practical conditions like thermal insulation [15]. Hence, it is important to smartly utilize silica aerogel to improve its engineering properties while without compromising porosity and thermal insulation properties significantly.

Currently available silica aerogel is mainly produced from organic silica sources or commercial water glass. For instance, tetrathoxysilane (TEOS) and methyltrimethoxysilane (MTMS), are relatively expensive and contain high embedded energy [5]. Meanwhile, commercial water glass is conventionally manufactured by reacting sodium carbonate (Na_2CO_3) with quartz sand in the molten state at 1300 ~ 1600 °C [16]. Therefore, exploring a cost-effective and environmentally friendly method to produce silica aerogel is of great interest [17,18], especially considering the sustainability development and environmental impact [19]. For the silica precursor, the silica produced by dissolving the mineral olivine in waste acid has lower energy requirements than conventional methods which include a spray pyrolysis (1200–1600 °C) process. In our previous research [20-23], it was shown that silica produced from olivine at 50–90 °C had a purity higher than 99% and a specific surface area between 100 to 400 m^2/g, which is much higher than normal silica [24], while the cost and CO_2 emission are much lower. Thus, the obtained nano-silica can react rapidly with sodium hydroxide (NaOH) to produce low modulus (SiO_2/Na_2O) sodium silicate at ambient pressure and low temperatures, thanks to its high surface area and reactivity. Thus, applying olivine-derived sodium silicate as a precursor instead of organic silica source (TEOS or TMOS) or commercial water glass can help to significantly reduce the energy consumption to produce aerogel.

In the past few years, several studies were focusing on the silica-cellulose composite aerogel (SCA). For example, Demilecamps et al., [25] explored the possibility of impregnating silica into the cellulose aerogel scaffolds via molecular diffusion and forced flow, with a final supercritical drying. The resulting composite aerogel showed a higher Young's modulus and lower thermal conductivity compared to the original cellulose aerogel. Zhao et al., [26] investigated the multiscale assembly of super-insulating silica aerogels within silylation nano-cellulosic scaffolds. It was demonstrated that the novel composite aerogel had low thermal conductivity and improved mechanical strength. However, most of these studies prepared silica-cellulose aerogel by forming cellulose aerogel first and with organic silica source. To be specific, the cellulose scaffold needs to be prepared first and later impregnated with silica components from sols derived from organic precursor.

Therefore, it is interesting to explore methods to prepare silica-cellulose aerogel from the sol-gel process of green sodium silicate and impregnate cellulose fibers in the silicate sol. Table 1 lists several typical synthesis methods mentioned in recent literatures using water glass. As can be seen, most of the studies investigate the cellulose hydrogel immersed in commercial water glass with a high modulus (3.3) and then used acid to form silica nanoparticles, followed by supercritical drying. However, it was found that with the cellulose nanofibers in silica hydrogel, the hydrogel can withstand the safer and more cost-effective freeze drying to obtain the aerogel. Hence, the conventional supercritical drying could be avoided.

In this study, the cellulose nano-fibrils are introduced in the inorganic and cost-effective silicate sol-gel process. The hydroxyl groups of the polymerized silicate sols during condensation and gelation can react with the –OH groups on chains of the cellulose fibers, leading the two materials chemically attached with each other and form composite hydrogel. The final silica hydrogel was reinforced with the cellulose fibers. Since the purpose of using

Table 1
Production methods and properties of silica-cellulose aerogel using commercial water glass as precursor.

Literatures	Synthesis methods	Drying method
Liu et al., [9]	Cellulose hydrogel film dipped in water glass followed by ethanol and sulfuric acid catalyst.	Supercritical drying
Demilecamps et al. [27]	Cellulose-8%NaOH-1%ZnO suspension was added with sodium silicate solution to form cellulose gel. Acid was used to form silica particles in the composite aerogel.	Supercritical drying
Sai et al., [28]	Bacterial cellulose hydrogels immersed in sodium silicate solution to gel and followed by acid catalyst.	Freeze drying

the composite aerogel was to explore the possibility to apply for thermal insulation, the volume stability and cost-effective of the developed aerogel are significantly important. Therefore, hydrophobization of the silica-cellulose composites aerogel is necessary to avoid water penetration into the hydrophilic aerogel, to increase the volume stability and service life of the composite aerogel. Because the wetting–drying processes caused by moisture in the environment can damage the pore structure of the composite aerogel, leading to the collapse of the structure. Hence, TMCS was applied for hydrophobization by chemical vapor deposition. The schematic diagram of the mechanism is shown in Fig. 1.

Overall, a facile synthesis of silica-cellulose aerogel (SCA) is presented by incorporating renewable cellulose nano-fibrils into the low-cost silicate sol-gel process and freeze-drying the composite gel. Olivine silica is used to prepare the green sodium silicate precursor. The procedure is promising to prepare sustainable SCA with ultra-low density, low thermal conductivity and relatively higher mechanical properties than plain cellulose aerogel.

2. Experimental

2.1. Starting materials

Olivine silica used for aerogel preparation was provided by Eurosupport. The specific surface area, pore volume, pore size, particle size and silanol content of olivine silica are shown in Table 2. The amorphous state of olivine silica is visible by X-ray diffraction pattern as shown in Fig. S1 (a). The olivine silica has a surface area of around 274 m^2/g, indicating a fast reaction rate with sodium hydroxide. Moreover, the pore volume and pore size are both high, reaching 0.72 cm^3/g and 10 nm, respectively. The silanol content of olivine silica reaches 8 ~ 20 OH/nm^2, which is far beyond the commercial fumed silica and pyrogenic silica, which have a silanol content of 3 ~ 4 OH/nm^2 [29].

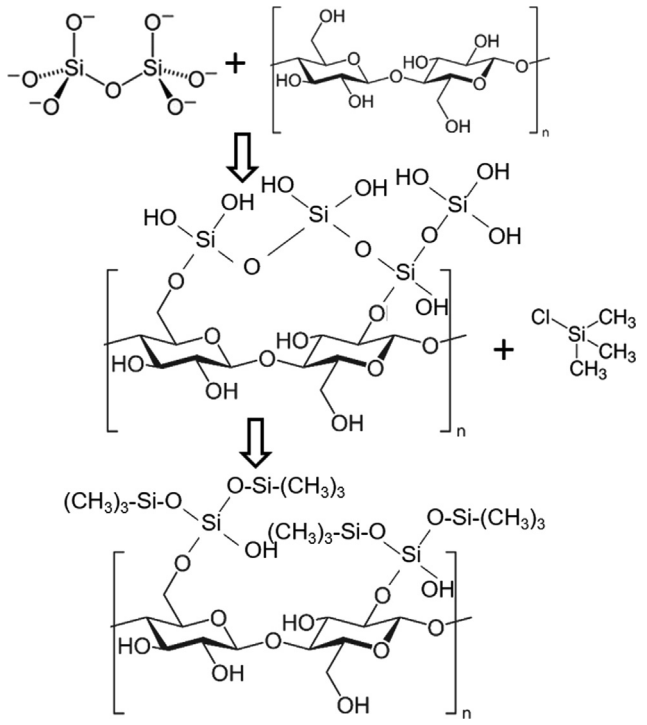

Fig. 1. Schematic diagram of mechanism for SCA preparation and TMCS modification.

Olivine-derived sodium silicate with a modulus of 1.5 with 8% silica content was prepared by reacting the olivine silica with sodium hydroxide (NaOH) solution at 80 °C for 2 h. The recipe for preparation of sodium silicate is presented in Table 3. The practical modulus was determined by using X-ray florescence. As observed in Fig. S1 (b), the mass percentage of dissolved silica in sodium hydroxide was around 99.73%, indicating a nearly completely dissolution of olivine-silica. The undissolved silica particles have limited influence on the quality of prepared sodium silicate due to the very small fraction in sodium silicate (0.27%). The pH of the prepared sodium silicate solution was 12.98, which is slightly lower than that of the commercial water glass (13.69).

In order to determine the types of silicate species in olivine sodium silicate, ^{29}Si NMR test was carried out to measure the silicate state and the results are shown in Fig. 2. The sharp peak at −72 ppm represents the existence of Q^0 monomers, while Q^1 dimers and Q^2 trimers at c.a. −80 and −82 ppm can also be observed. Meanwhile, a moderate number of Q^2/Q^3 groups can be observed at around −86 to −90 ppm. No Q^4 sites can be observed, with the locations lower than −100 ppm, which means all the silica in Q^4 form is dissolved in solution.

For the olivine sodium silicate, a significant peak at −72 ppm indicates most of the silicate structure is monomers silicate. While the minor peaks at the chemical shifts of around −80 ppm show a less extent of Q^1 and Q^2 sites for silicate. Trace number of Q^2/Q^3 sites can be observed at −87 to −90 ppm, indicating few percentage of highly polymerized silicate. However, compared to the NMR analysis of commercial water glass with a modulus of 3.3, there is significant difference, indicating a much higher polymerized silicate species. This is because commercial water glass production includes a silica sand at a much higher temperature of 1300 to 1600 degree of calcination with sodium carbonate (Na_2CO_3), so more silicates are supposed to polymerize in solid solutions and thus more Q^4 silicate species are expected. However, more energy is also supposed to be involved in this process which is not sustainable and green. Therefore, the difference in structure of silicate species in sodium silicate solution may influence the properties and microstructure of the resulting aerogel.

Water suspensions of two kinds of cellulose nanofibrils (CNF) were provided by Sappi, the Netherlands. CNF1 has a Fine S of 94% and Fine P of 4.6% while CNF2 had a Fine S of 48% and Fine P of 23.5%. The cellulose was derived from wood pulp that has been sourced from sustainably managed forests. The CNFs were prepared by the mechanical super-milling method with the α-cellulose source in the form of a white gel. The original concentration of CNF1 and CNF2 were 2.7 wt% and 3.1 wt%, respectively, which was determined by heating the raw CNF suspension at 105 °C until constant mass and then calculate the concentration of solid content in the suspension. The pH of the CNFs was between 6.5 and 7.5. A good dispersion of cellulose fibers is critical to utilize its full benefits. The two CNFs were mixed for 30 min at 2000 rpm with a high shear mixer (Model L5M, high shear laboratory mixer, Silverson Machines Ltd.) to improve their dispersion until showing efficient thickening effect with a cream-like appearance. The SEM and TEM images of these two CNFs are presented in Fig. 3. The diameter of the two kinds of nanofibers are similar, however, the length of these two fibers were different, ranging from a few micrometers to tens of microns. The surface charge of CNF1 and CNF2 measured by zeta potential was −52.5 mV and −40.5 mV, respectively. The properties of the used CNF1 and CNF2 are shown in Table S1.

Other chemicals used were sodium hydroxide pellets (NaOH), n-heptane (C_7H_{16}), ammonia solution ($NH_3{\cdot}H_2O$, 25%), trimethylchlorosilane (C_3H_9SiCl, >99%) and Amberlyst 15 hydrogen form (H^+ cation exchange resin) for preparation of silica-cellulose composite aerogel.

Table 2
Properties of olivine silica.

Properties	Surface area (m^2/g)	Pore volume (cm^3/g)	Average Pore size (nm)	Average Particle size (μm)	Silanol content (OH/nm^2)
Olivine silica	274 ± 14	0.72 ± 0.05	~10	~17	8 ~ 20

Table 3
Recipe of water glass preparation from olivine silica and sodium hydroxide.

Olivine silica (g)	Sodium hydroxide (g)	Distilled water(g)	Temperature (°C)	Theoretical modulus	Measured modulus	SiO_2 concentration (%)
9	8	95.5	80	1.50	1.45	7.9

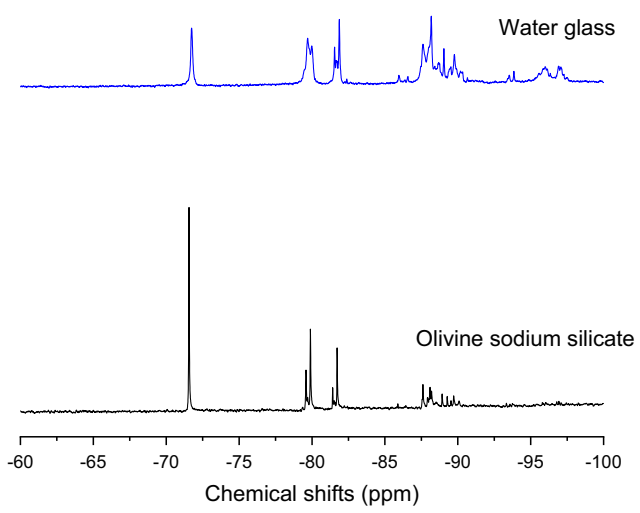

Fig. 2. Si^{29} NMR spectra of olivine derived sodium silicate and commercial water glass.

2.2. Preparation of silica-cellulose composite aerogel

The 8% as-prepared olivine sodium silicate was passed through ion exchange resin to obtain silicic acid, with a final pH of 2.0 ~ 2.5. Then, 25 mL of silica sol was mixed with CNFs in a beaker for 60 min at room temperature. Later, the pH of the silica-cellulose composite suspension was increased to 5.0 ~ 5.5 by adding 1 M ammonium hydroxide to accelerate the gelation process. Afterwards, the suspension was placed into a mold to cast the silica-cellulose hydrogel. For all the hydrogels, the gelation times were around 20 min. The composite hydrogel image is shwon in Fig. S2, showing trasnparent and homogeneous gel. Lastly, the mold was sealed air tight with a plastic film. After 1 day aging at room temperature, the silica-cellulose composite hydrogel was freeze-dried. Specifically, the hydrogel was immersed in liquid N_2 at a temperature of − 196 °C. The frozen sample was dried in a freeze dryer (Alpha 2–4 LD plus from Martin Christ, Salmenkipp) under the following conditions: ice condenser = − 57 °C; vacuum ≤ 0.1 mbar; and time = 48 h. For the hydrophobic treatment of SCA, the as-prepared composite aerogel was treated by thermal chemical vapor deposition with trimethylchlorosilane (TMCS). Magnesium chloride saturated solution was poured into a vacuum desiccator for regulating relative humidity at range from 35% to 65% for 24 h. SCA was placed in a 200 mL beaker, while a 3 mL of TMCS was inserted in another 10 mL beaker. The smaller beaker containing TMCS was placed inside the 200 mL beaker. This double beaker setup was placed in the desicator and was designed to prevent direct contact of the aerogel with TMCS. The 200 mL beaker was sealed with a cap and placed in an vaccum oven at 160°for 1 h. Unreacted silanes were removed by keeping the aerogel in vacuum drying oven until the pressure reached 0.03 mbar or less. The prepared hydrophobic SCA was ready for characterization. The schematic diagram of the preparation of silica-cellulose composite aerogel is presented in Fig. 4.

2.3. Preparation of pure cellulose areogel

Pure cellulose aerogel was prepared according to the previous researches as reference [30,31]. The CNF1 and CNF2 suspensions were first diluted with distilled water to a concentration of 0.55% and 0.60%, respectively. The diluted suspensions were continuously stirred at 480 rpm at 20 °C for 30 min using a magnetic stirrer. Then, the diluted suspension was moved into a cylindrical plastic mold with a diameter of 10 mm and a height of 20 mm. Afterwards, the assembly was frozen dried with liquid nitrogen and then moved to a freeze dryer to extract the solvent for 2 days. The recipe of all the six samples is shown in Table 4.

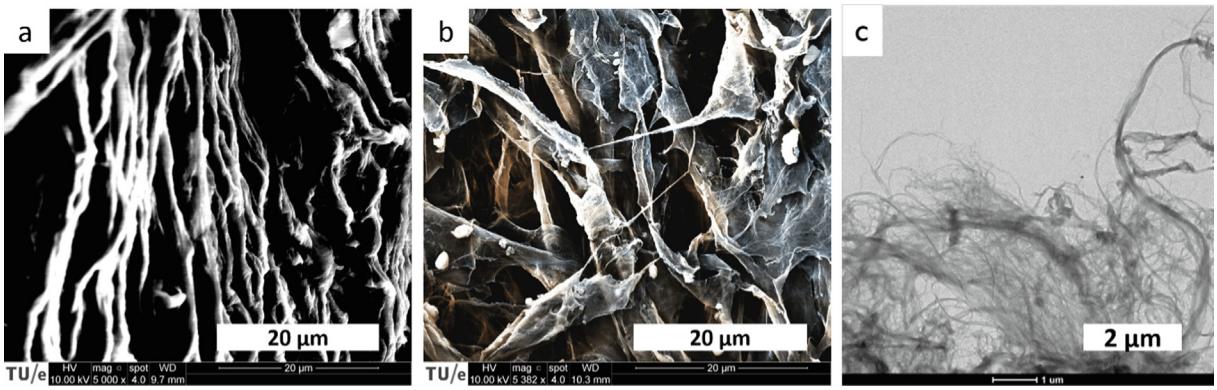

Fig. 3. SEM of (a) CNF1 and (b) CNF2 and (c) TEM of CNFs.

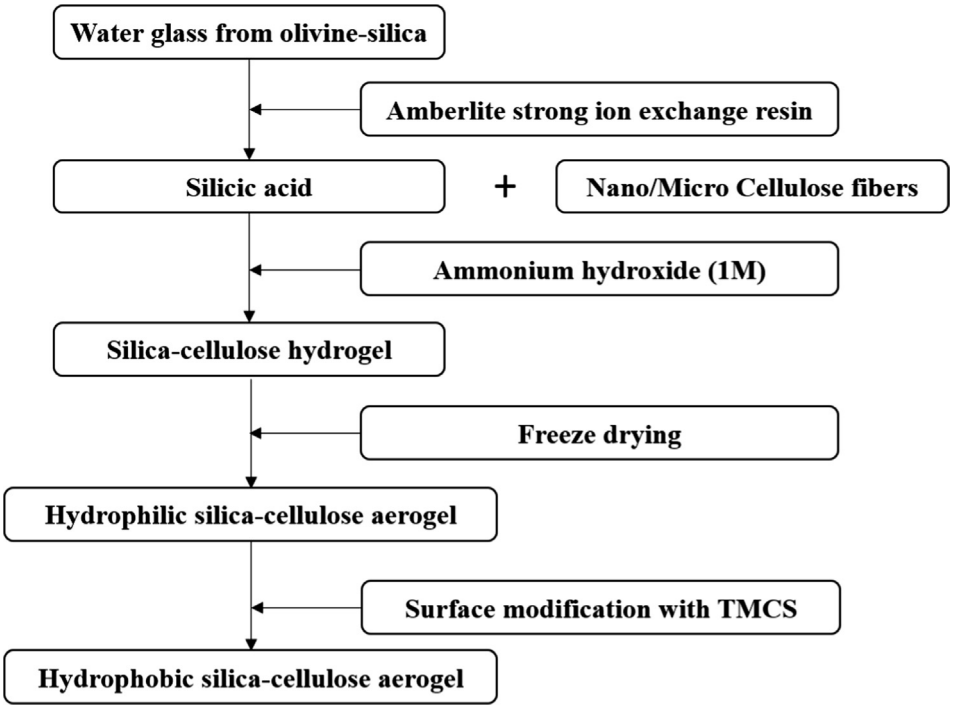

Fig. 4. Schematic diagram of the preparation of silica-cellulose composite aerogel.

Table 4
Recipe design of the investigated aerogel samples in this study.

Groups	CNF1 (mL)	CNF2 (mL)	8% Silica sol (mL)	Distilled water (mL)	TMCS modification
SS-CNF1	5	0	25	0	N*
SS-CNF2	0	5	25	0	N
SS-CNF1-M	5	0	25	0	Y*
SS-CNF2-M	0	5	25	0	Y
NCA1	5	0	0	25	N
NCA2	0	5	0	25	N

*N = No, *Y = Yes

2.4. Characterization of the composite aerogel

The skeletal density of the prepared silica-cellulose aerogels was determined with a Helium pycnometer (AccuPyc II 1340 Micromeritics). The bulk density of the as-prepared SCAs was determined by using the bulk volume and mass of the prepared samples. Based on the two densities, the porosity of the SCAs was determined according to:

$$\Phi = (1 - \frac{\rho_b}{\rho_s}) \times 100 \quad (1)$$

Where ϕ is the porosity of the tested aerogel, ρs the skeleton density of the tested aerogel, ρ_b the bulk density of the tested aerogel.

Water suspension of CNF was prepared for TEM analysis. The suspension was diluted to 1% of original concentrated CNF solution. A 200 mesh Cu grid covered with a continuous carbon film was used to support the CNF sample. FEI Tecnai 20 Sphera instrument with a LaB6 filament was operated at an accelerating voltage of 200 kV to observe the microstructure of CNF.

The mechanical property of the SCAs with a cylindrical shape (10 mm diameter × 20 mm height) was tested in an MTS Criterion equipped with a load cell of 200 N at a speed of 1 mm/min to ε = 80% of its original height. The thermal conductivity of the SCAs was determined with TPS-instruments (Hot disk). The water contact angle (CA) measurements using sessile drop technique was used to determine the hydrophobicity of SCAs (Dataphysics Contact Angle System, TBU 90E). The volume of the Milli-Q water droplet used for the contact angle test was 3.000 μL. The final results correspond with the average measured CA of five droplets on the surface of SCAs. The margin of error was defined as the 95% confidence interval of the five measurements.

The microstructure of the SCAs was observed with scanning electron microscopy (SEM), by using a JOEL JSM-5600 instrument at an accelerating voltage of 15 kV. The thermal stability of the SCAs was determined with thermogravimetric analysis by using a NETZSCH STA449-F1 instrument with a heating rate of 5 °C/min under air atmosphere. Chemical bonds in the SCAs were detected by using a Varian 3100 Fourier-transform infrared spectroscopy (FTIR) with wavenumbers ranging from 4000 to 400 cm^{-1} at a resolution of 2 cm^{-1}. The specific surface area and pore size distribution were measured by nitrogen physisorption, which was carried out with a Tristar 3000 Series micrometer employing nitrogen at 77 K. The samples were pretreated by nitrogen gas flow with a heating rate of 10 °C/min and heated up at 80 °C for 4 h to remove moisture. Solid state MAS NMR spectra were carried out using a Bruker Advance 400WB spectrometer. The ^{29}Si NMR spectra were collected at 79.5 MHz on a 7 mm probe, with a pulse width of 6.5 μs, a spinning speed of 15.9 kHz and a relaxation delay of 10 s.

3. Results and discussions

3.1. Microstructural analysis

3.1.1. SEM analysis

The SEM of SCA with different cellulose nanofibrils and modification are shown in Fig. 5. The SCA shows a random distribution of silica and cellulose fibers, due to the heterogenous nature of cellulose fibers and because silica aerogel was also attached to these randomly distributed fibers. As observed in Fig, 5, the silica aerogel has a relatively strong affinity with cellulose fibers. For SS-CNF1, the nanofibers were crossly linked within the silica aerogel structures; the silica surface was very smooth and showed a more homogeneous structure. This silica microstructure was rather different from those of conventional silica-cellulose aerogels using commercial water glass as shown in Table 1, which implies silica monodisperse spherical particles inside the cellulose matrix (Liu et al., 2013; Demilecamps et al., 2014). Therefore, the developed SCA in this study could have a higher surface area and enhanced homogeneity. As can be seen from the NMR analysis of silica precursors in section 2.1, the commercial water glass contains more highly polymerized silicate (Q3/Q4) than olivine sodium silicate, which may be the reason of the difference in the silica morphology. Most of the micrometer-sized pores (20 ~ 50 μm) in original cellulose aerogel [31] (Fig. S3) are filled with silica aerogel, making it a more compacted composite than plain cellulose aerogel. However, there still exists a few pores with the size of 10 ~ 20 μm between cellulose fibers. For SS-CNF2, the cellulose fibers are slightly wider and the less homogeneous than SS-CNF1 due to the higher fraction of coarser cellulose nanofibrils in the raw material.

After surface modification of SCA by TMCS reagent, the shape of the cellulose fibers remained the same while the surface of silica aerogel particles became rougher and clustery, which is in accordance with the BET results shown later, showing lower surface area of SS-CNF1-M. This change in morphology was expected since the Si-O–H group was substituted by the Si-O-Si$(CH_3)_3$ group as presented in Fig. 1.

The plain cellulose aerogel contains the macropores between cellulose fibers with the size of around 20 ~ 50 μm, which was rather large compared to that of silica aerogel (10 ~ 20 nm) and SCA. Therefore, this loose structure makes plain cellulose aerogel less thermal insulating due to the air molecules can still move freely in the micron-sized pores and promote gaseous heat transfer via convection. Therefore, the silica-cellulose composite aerogel can overcome this drawback by incorporating silica aerogel in the pores to decrease gaseous heat transfer and even improve the thermal stability of cellulose fibers.

3.1.2. Specific surface area and pore structure

The physisorption isotherm and pore size distribution of SCAs from nitrogen physisorption test are presented in Fig. 6. The specific surface area, total pore volume and average pore size of the developed SCAs are shown in Table 5. Pure cellulose aerogel has a SSA_{BET} of around 100 ~ 200 m^2/g, while silica aerogel has a SSA_{BET} of 600 ~ 700 m^2/g (See Fig. S4). Table 4 indicates that the specific surface area of all the composite aerogels increased significantly

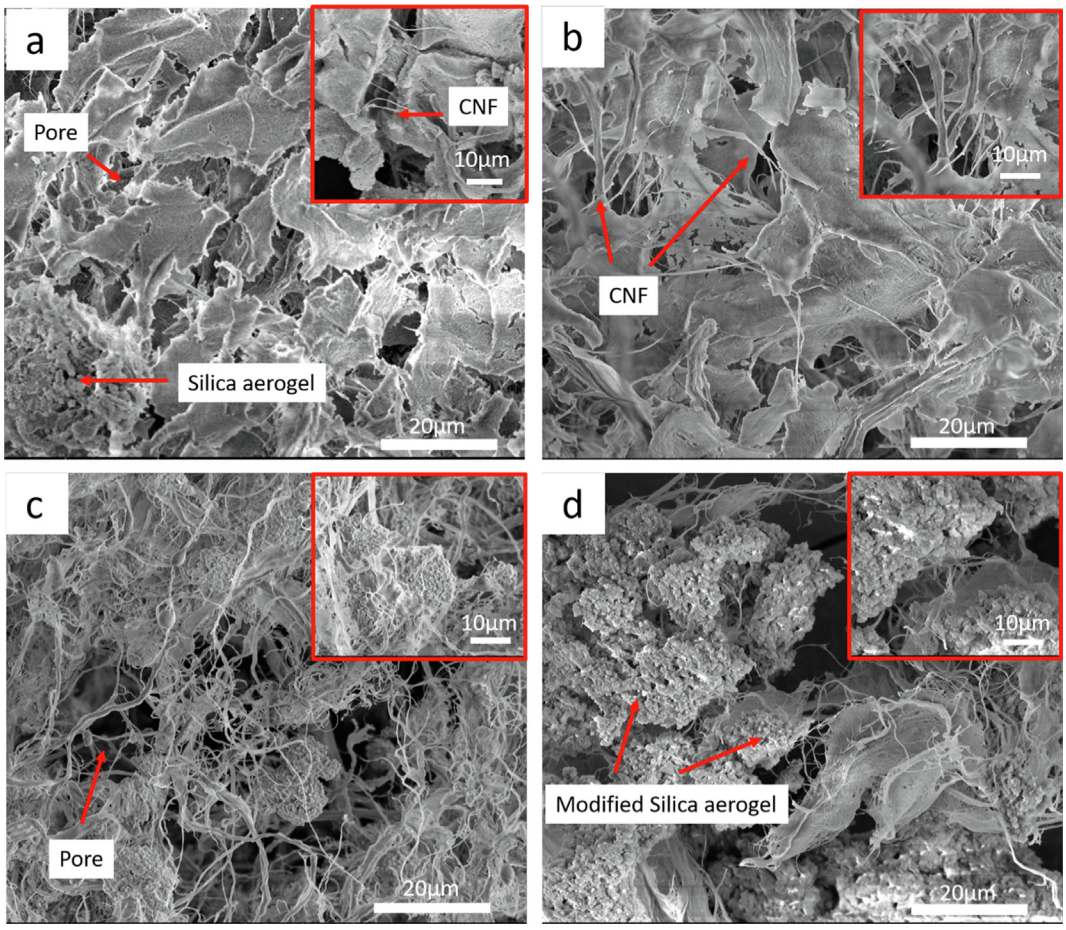

Fig. 5. SEM of SCA with different CNFs and surface treatment: (a) SS-CNF1 (b) SS-CNF2 (c) SS-CNF1-M (d) SS-CNF2-M.

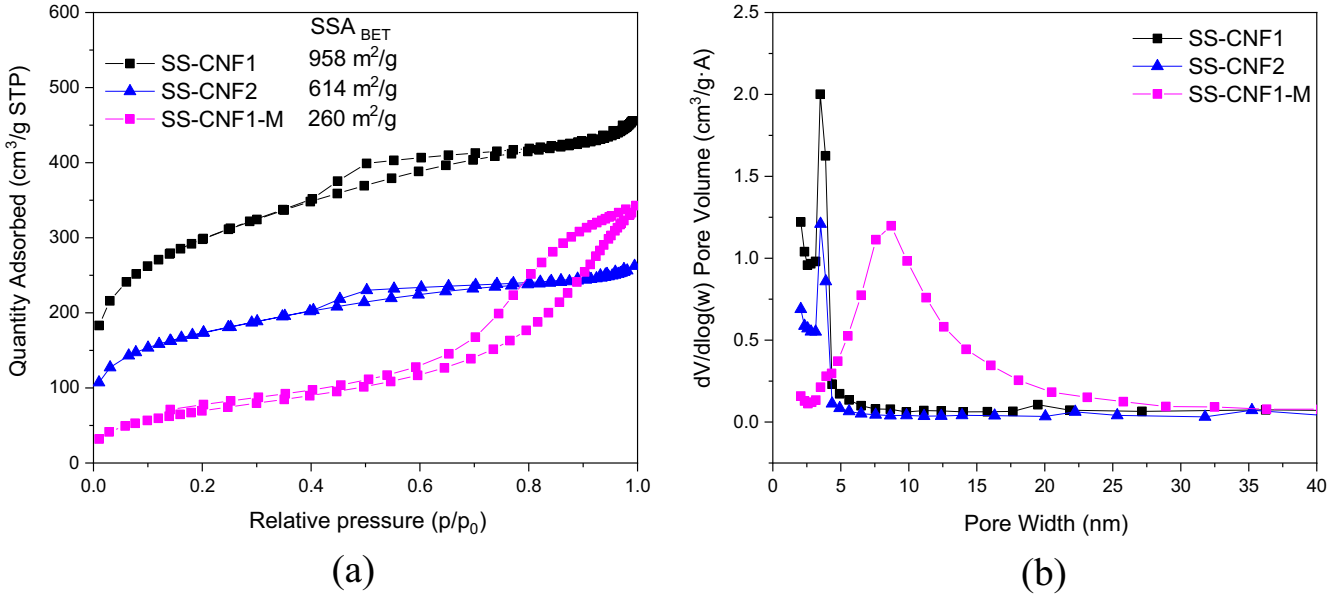

Fig. 6. Nitrogen physisorption isotherm (a) and pore size distribution (b) of the as-prepared SCAs.

Table 5
Specific surface area, total pore volume and average pore size of the developed SCAs and comparison with silica aerogel and cellulose aerogel.

Groups	BET surface area (m^2/g)	Total pore volume (cm^3/g)	Average pore width (nm)
SS-CNF1	958 ± 12	0.53 ± 0.01	3.51 ± 0.11
SS-CNF2	614 ± 10	0.29 ± 0.01	3.52 ± 0.19
SS-CNF1-M	260 ± 9	0.55 ± 0.02	7.94 ± 0.36
Cellulose aerogel	200 ~ 300	0.24 ~ 0.30	10 ~ 30
Silica aerogel	600 ~ 700	2.5 ~ 3.0	10 ~ 20

compared to cellulose aerogel, suggesting the existence of nanostructured silica aerogel filling in the surface and pores of the cellulose matrix.

Table 5 shows the SSA of SS-CNF1 and SS-CNF2 are much larger than that of pure cellulose aerogel and are similar to pure silica aerogel, reaching 958 m^2/g and 614 m^2/g, respectively. This result probably relates to the silica 3D network that has a higher surface area and thus leads to the increased surface area in the composite aerogels. The SSA of SS-CNF1 is also much higher than other researchers' work, which obtain a SSA of silica-cellulose aerogel reaching only 340 m^2/g and 150 m^2/g, respectively [9,32]. This phenomenon can be explained by the difference in the silicate structure as shown in the NMR test for the silicate precursor. It may indicate that low modulus silicate could form smaller silica particles inside the cellulose nanofibrils and increase the surface area. The physisorption isotherms of SS-CNF1 and SS-CNF2 present a typical Type IV isotherm, with a relatively small hysteresis, which is due to the narrow pore size distribution, with uniformly distributed pores below 4 nm. (See Fig. 6 (b)). At p/p_0 = 0.1 of the nitrogen isotherm exist a slight leap, indicating a moderate amount of micro-porosity, which may contribute to the large surface area as well. Therefore, this indicates silica aerogel covers the surface of cellulose fibers, thus changing the randomly distributed nanopores of cellulose to uniformly distributed nanopores of silica aerogel.

The isotherm and pore structure of SCA changed significantly after TMCS modification, as shown in Fig. 6. The isotherm changed to a non-typical Type IV isotherm, indicating hydrophobic modification of aerogel result in a change in the pore size distribution. The relatively large hysteresis was caused by the broad pore size distribution with most pores ranging from 5 nm to 20 nm and concentrated in 8 nm. The larger pore sizes could be attributed to $-CH_3$ groups attached on the surface of silica, resulting in swelling of pores due to the repulsive force between the $-CH_3$ bonding.

3.1.3. FTIR spectra

The FTIR spectra of reference NCA and SCA before and after TMCS modification are shown in Fig. 7. The reference NCA spectra present typical bands of cellulose fibers, for instance, the hump at 3340 cm^{-1} and 1632 cm^{-1} suggesting O–H stretching and bending, and the sharp peak at 1053 cm^{-1} indicating C-O-C skeletal vibrations. Meanwhile, the characteristic peaks of C–H bending, C = C and C = O stretching are visible at 1376, 1310, and 1253 cm^{-1}, respectively.

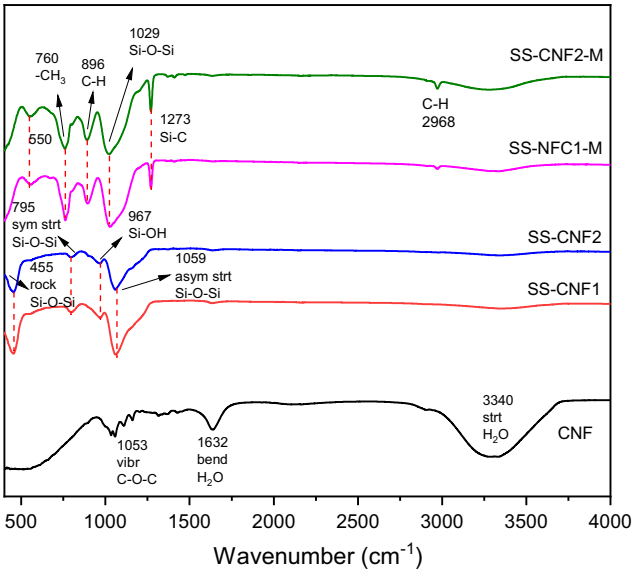

Fig. 7. FTIR of silica-cellulose aerogel before and after TMCS hydrophobic modification.

The SCA before hydrophobic treatment has typical Si-O-Si peaks, corresponding to 1059 cm^{-1} (asymmetrical stretching vibration), 795 cm^{-1} (asymmetrical stretching vibration) and 455 cm^{-1} (rocking vibration). Also, the Si-O–H bond can be observed at 967 cm^{-1}, showing the large amounts of hydroxyl groups on the silica surface that are available to react with the TMCS reagents for hydrophobic treatment. Minor amounts of H-O–H groups can be observed at 1632 cm^{-1} and 3340 cm^{-1} corresponding to bending vibration and stretching vibration of physically bound water. It shows the water was mostly removed through freeze drying. However, due to the hydrophilic nature of unmodified SCA, moisture in the air can be easily absorbed on the surface of aerogel, thus hydrophobic modification was necessary to resist water penetration that can damage the structure of SCA.

Due to the modification with TMCS, the SCA becomes hydrophobic. TMCS has a Si-Cl bond that can react with the silanol groups of the unmodified SCA. For SS-CNF1-M and SS-CNF2-M, the characteristic peaks of the Si-C bonds are visible at 896 cm^{-1} and 1273 cm^{-1}. Also, the bending vibration of the $-CH_3$ group appears at 760 cm^{-1}. Furthermore, the characteristic peak of the Si-OH bond at 967 cm^{-1} disappears after surface modification, which means the silanol group was substituted by the $Si\text{-}O\text{-}Si(CH_3)_3$ group (896 cm^{-1}, 760 cm^{-1}).

The intensities of Si-C and $-CH_3$ bands of the two SCA are slightly different, even though the volume of TMCS used for surface modification remains the same. Hence, as discussed before, the BET result show that SS-NFC has a significantly higher surface area than SS-MFC. Therefore, the TMCS usage for NFC should be higher than that of MFC to reach the same level of trimethyl silyation, leading to the reduced intensity of Si-C and $-CH_3$ bands for SS-NFC.

3.1.4. TG/DTG analyses

The thermal gravimetry (TG) and differential thermal gravimetry (DTG) curves of SCA with different cellulose fibers and surface modification are illustrated in Fig. 8. The thermal decomposition of the reference NCA aerogel both consists of two phases. Firstly, the physical bound water to the surface of cellulose fibers evaporates before 105 °C. It can be observed the physical bond water was 4 wt% for NCA. The second phase of decomposition lasts from 250 °C to 375 °C, which was attributed to the burning of cellulose fiber. The carbon chain normally decomposes at around 300 ~ 350 °C. At this stage, most of the mass of the cellulose aerogel was lost. After heating from 375 °C to 1000 °C, the residual mass of the cellulose aerogel is carbon black, which is only 5 wt% for NCA. Therefore, pure cellulose aerogel can be vulnerable to higher temperatures and then loses the structural stability, consequently leading to a total collapse.

However, the SS-CNF1 and SS-CNF2 aerogels showed different decomposition phases and residual mass at 1000 °C, as shown in Fig. 8 (a). The amount of physical bound water for SS-CNF1 and CNF2 are higher than CNF1 and CNF2 samples, reaching 11.6% and 12.5%, respectively, indicating a more hydrophilic property. The mass loss of SS-CNF1 and SS-CNF2 between 250 ~ 400 °C was 9.36% and 15.57%, respectively. Also, it can be noticed that the peak position in the DTG curve for this temperature range was different for SS-CNF1 and SS-CNF2. For SS-CNF1, the peak situated at 345.5 °C, while for SS-CNF2 the peak shifted to 333.0 °C. The residual mass after 1000 °C of both samples showed a relatively high value due to the existence of silica, reaching 72.35% and 62.89%, respectively, indicating that the thermal stability of silica aerogel was much higher than that of cellulose aerogel. As observed from Table 6, the decomposition temperature of the DTG peak was increased due to the incorporation of silica, rising from 309 °C to 345.5 °C for CNF1 and to 333 °C for CNF2, respectively. Therefore, silica dosage can slightly improve the thermal stability of the composite aerogel.

After modification by TMCS, the physically bond water was significantly reduced for both SS-CNF1-M and SS-CNF2-M, showing the successful hydrophobic treatment. The decomposition temperature of cellulose fibers also increased to 331 °C and 329 °C for SS-CNF1-M and SS-CNF2-M, as compared to reference cellulose fibers. However, surface modification cannot further increase the thermal stability of the composite aerogel compared to hydrophilic SCA. The peak DT was still situated at around 329 ~ 331 °C.

3.2. Density and porosity of silica-cellulose aerogel

The skeletal density ρ_k, bulk density ρ_b and porosity ϕ of cellulose aerogel and silica-cellulose composites aerogel are shown in Table 7. The bulk density of the SCAs varied from 0.052 to 0.061 g/cm^3, which is in between the plain silica aerogel (~0.1 g/cm^3) and cellulose aerogel (~0.012 g/cm^3). This is because the silica aerogel was attached on the surface of cellulose fibers and thus increases the pure cellulose density, while the scaffold of cellulose aerogel provides an ultralight matrix for silica aerogel.

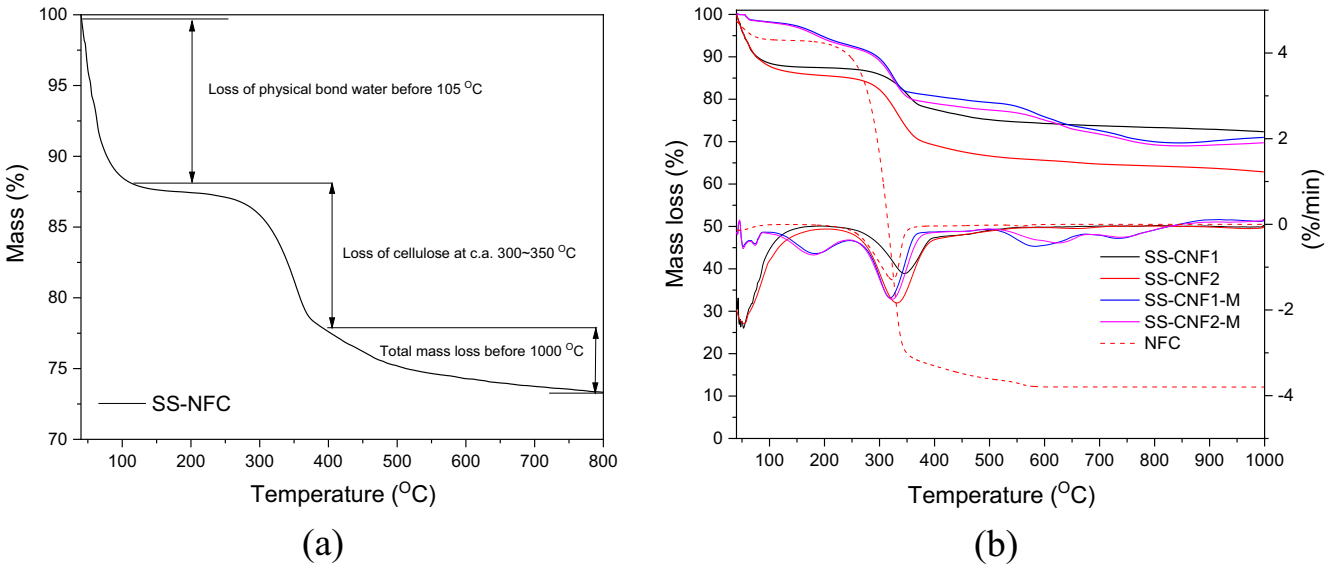

Fig. 8. Thermogravimeter analysis of (a) SS-CNF1 and (b) reference CNF and SCA of different cellulose fibers and surface modification.

Table 6
Decomposition temperatures of cellulose fibers of each group.

Groups	Initial cellulose decomposition T (°C)	Peak of cellulose decomposition T (°C)	End of cellulose decomposition T (°C)
SS-CNF1	249.5	345.5	410.0
SS-CNF2	248.6	333.0	408.5
SS-CNF1-M	260.6	331.3	390.6
SS-CNF2-M	261.3	329.3	391.6
NCA1	240.6	309.0	375.0

Table 7
Skeletal density, bulk density and porosity of the investigated aerogels.

Groups	Skeletal density (g/cm^3)	Bulk density (g/cm^3)	Porosity (%)
SS-CNF1	1.82 ± 0.02	0.054 ± 0.01	97.0 ± 0.01
SS-CNF2	1.78 ± 0.01	0.052 ± 0.01	97.1 ± 0.02
SS-CNF1-M	1.87 ± 0.03	0.061 ± 0.02	96.7 ± 0.01
SS-CNF2-M	1.85 ± 0.01	0.059 ± 0.02	96.8 ± 0.02
NCA1	1.53 ± 0.01	0.013 ± 0.01	99.1 ± 0.03
NCA2	1.51 ± 0.02	0.011 ± 0.02	99.3 ± 0.03
Silica aerogel	2.1	0.08 ~ 0.13	95 ~ 99

Thus, the density of SCA falls in the middle of the density of cellulose aerogel and silica aerogel, which was in line with the SEM and FTIR analysis. Pure cellulose aerogel obtains a much lower density than SCA, because silica aerogel (~0.1 g/cm^3) fills in the interparticle pores of cellulose nanofibrils (~0.02 g/cm^3). Also, the pore size of silica aerogel and cellulose aerogel was very different: silica aerogel has nanometer-sized *meso*-pores while for cellulose aerogel the pore size was tens of micrometers. Therefore, it is reasonable for SCA to have a higher density than that of cellulose aerogel, while it has a lower bulk density than silica aerogel.

It is also observed that the four types of SCAs have slightly different densities and porosities (Table 6). SS-CNF2 has the lowest density (0.052 g/cm^3) among all the SCAs, showing the highest porosity of 97.1%. However, the density of SS-CNF1 was similar to SS-CNF2 ones. Furthermore, the density increases after TMCS modification, indicating the replacement of –OH group by –Si $(CH_3)_3$ group can increase the density of SCA since it has a larger molecular mass. Although the density of SCA increases, the porosity only slightly decreases, indicating a minor influence of surface modification on the porosity of SCA.

It also can be observed that NCA1 has a slightly higher bulk density than NCA2. NCA1 contains more finer nanoscale fibers, so more fibers are in close contact with each other. The NCA2 has much longer fibers and thus the micrometer pores are much larger than for NCA1, resulting in a looser structure. Overall, the SCA composite aerogel has a lower bulk density than plain silica aerogel, while higher than that of reference cellulose aerogel.

3.3. Mechanical properties

The uniaxial compression results of the reference cellulose and SCAs are presented in Fig. 9. The mechanical parameters are summarized in Table 8. The stress–strain curves of the tested groups show three stages: a linear trend at very low strains (< 5%), an increased slope at higher strains, and a final densification because of the collapse of the fibers pore walls. The tests were all performed until the sample was about to break at around 80% strain. For the reference CNF aerogel, the curve was typical for aerogel prepared from cellulose fibers at a very low concentration of 0.60% and 0.55% in aqueous solution [30]. The main deformation was due to the bending of the fibers and collapsing of the pores, while the

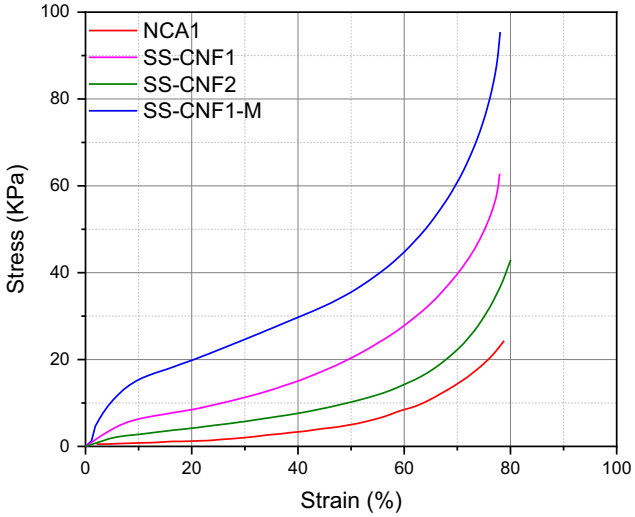

Fig. 9. Stress–strain uniaxial compressive curves of SCA and reference NCA.

Table 8
Young's modulus *E*, fracture stress σ^* and strain S^* for reference cellulose/silica aerogel and SCAs.

Groups	E (KPa)	σ^* (KPa)	S^* (%)
NCA	35.3 ± 0.4	29.8 ± 0.1	84.3 ± 0.3
SS-CNF1	80.5 ± 0.2	62.8 ± 0.2	78.0 ± 0.3
SS-CNF2	62.8 ± 0.2	42.8 ± 0.1	84.1 ± 0.1
SS-CNF1-M	122.2 ± 0.3	95.4 ± 0.1	78.1 ± 0.2

compressive strength was provided by the physical cross-linking fibers and hydrogen bonds [25]. When the strain reaches higher values, the micrometer-sized pores were compressed and broken, leading to the densification of the pores resulting in load bearing of the samples. As can be seen from Table 8, the Young's modulus and compressive strength of the reference NCA was very low, reaching only 29.8 kPa. This is attributed to the ultralow density and high porosity and weak cellulose strength of the cellulose aerogels. The plain silica aerogel shows a very low stress value at low strains, according to silica aerogels prepared by other researchers, which is due to the brittleness of silica aerogel and lack of flexibility that lead to the limitation to reach higher strain. [33]. Although differences exist among the accurate stresses of different silica aerogels, the nature of brittleness of the silicon-oxygen bond is widely acknowledged.

However, cellulose-silica composites aerogels presented a relatively clear improvement in Young's modulus and stress–strain curves, compared to both reference silica aerogel and cellulose aerogel. The fracture stress of SS-CNF1 and SS-CNF2 reached 62.8 and 42.8 KPa, respectively. The improvement in compressive strength was firstly due to the increase in density and decrease in total porosity. As more silica aerogel was impregnated in the pores of cellulose fibers, the density was increased thus also the strength. Another important reason was the covalent bond between cellulose changed to silicon-oxygen bond as seen in FTIR analysis. In fact, the Si-O bond is a very strong bond (452 kJ/mol), however not ductile due to the silicon-oxygen tetrahedron. Therefore, it is interesting to compensate for this shortcoming by combining cellulose fibers which can improve the ductility of the composite materials. At higher strain when the interpore of cellulose fibers is condensed, the impregnated silica can also support the pores from collapsing. Therefore, the SCAs have improved mechanical properties.

After surface modification, the density of SCA further increases and the strength of SS-CNF1-M increases significantly, reaching 95.4 kPa. The synergy of $-CH_3$ groups with cellulose silica aerogel matrix provides stiffer and more ductile aerogel [34]. The repulsive forces between $-CH_3$ groups further increase the compressive strength of SCAs. Therefore, surface modification of SCAs can improve the mechanical properties of SCAs significantly.

3.4. Thermal conductivity

The thermal conductivity of SCAs and reference cellulose and silica aerogels are shown in Table 9. The reference silica aerogels possess thermal conductivities of 0.016–0.018 W/(m·K) at room temperature and pressure, which are known to be super-insulating materials. The reference NCA1 and NCA2 have much higher thermal conductivity of 0.036 W/(m·K) and 0.038 W/(m·K), respectively. Although cellulose aerogel has very low bulk density (~0.01 g/cm^3), they contain numerous micron-sized open pores inside the aerogel, which cannot immobilize the air inside. The silica aerogel, however, has nanometer-sized open pores of around 5 ~ 20 nm. These tiny mesopores can immobilize the air movement inside the nanopores. The mean free path of air is 68 nm at ambient pressure and room temperature. Due to the Knudsen effect, the movement of air molecules was restricted and thus the thermal conductivity was significantly decreased and even lower than air [12].

For SS-CNF1 and SS-CNF2, the silica aerogel with lower thermal conductivity filled the micron-sized pores of the cellulose aerogel and covered the surface of the cellulose fibers as well. Thus, the thermal conductivity was reduced to 0.023 ~ 0.026 W/(m·K). These results also support the conclusion that the silica component was successfully incorporated into the matrix of cellulose fibers. However, the thermal conductivities of SCA were higher than that of plain silica aerogel. This is due to the remaining macrospores (cannot restrict air movement) inside the composite aerogel which are not fully occupied by silica aerogel and due to the increased density of SCA increases the phonon conduction through the skeleton network of silica and cellulose fibers.

There is also a slight difference among these four SCAs samples in terms of thermal insulation properties. SS-CNF1 has the thermal conductivity reaching 0.026 W/(m·K). While for SS-CNF2, this value decreases to 0.023 W/(m·K), most probably because of the difference in bulk density, as shown in Table 8. It is noticed that surface modification increases the thermal conductivity for both SS-CNF1 and SS-CNF2. The reason can be that more $-CH_3$ groups are attached to the silica aerogel which can increase the density of silica components in these samples. Also, the pore size of silica was bigger and randomly distributed after modification as discussed in BET analysis. Above all, the thermal conductivity of SCAs can reach a very low value which is desirable in thermal insulation fields. Since the composite aerogel can obtain low thermal conductivity and high thermal stability at the same time, it has the advantage over traditional insulation materials, for instance, styrene foam (0.4 W/(m·K)) and asbestos (0.08 W/(m·K)).

3.5. Hydrophobicity

The water contact angle of SCA with surface modification by the TMCS/heptane reagent solution is shown in Fig. 10. For the original SS-CNF1 and SS-CNF2, the Mill-Q water was immediately absorbed into the matrix due to the hydrophilic nature of the Si-OH bond and also due to the numerous micron-sized pores of hydrophilic cellulose fibers ($-CH_2$-OH bonds in cellulose), which makes the measurement of the water contact angle impossible. Contrariwise, as observed from Fig. 10, the water contact angle was very high for both SS-CNF1-M and SS-CNF2-M, reaching an average water contact angle of 137.0° and 140.4°, respectively, indicating their high hydrophobicity. Hydrophobicity was classified by a water contact angle above 90°. In addition, Fig. 10 (c) and (d) show that the water droplets stand on the surface of cylindrical and cubic composite aerogel without penetration.

The surface modification method is in accordance with other researchers using silane containing materials [35-37]. The high level of hydrophobicity can improve the durability of SCAs applied in the indoor environment because the moisture in the air can constantly penetrate the matrix of hydrophilic SCA leading to the wet-drying shrinkage of silica aerogel or even corruption of the cellulose fibers. The deterioration of the pore structure of SCA can result in significant increase of thermal conductivity, leading to the loss of thermal insulating performance. Therefore, surface silylation treatment can further prolong the service life of SCA. Also, thanks to its high thermal insulation and thermal stability, it could be an ideal candidate for interlayer thermal insulation material.

3.6. Sustainability

A significant motivation and potential advantage of using waste olivine silica to synthesize aerogel is the reduction of the carbon emission associated with the silica aerogel synthesis. In most cases, commercial water glass is used as the precursor. However, commercial water glass that is prepared using hydrothermal treatment has a CO_2 emission of 1.514 tCO_2/t [38], and the detailed energy use is presented in Table 10. The traditional hydrothermal method uses silica sand and sodium hydroxide as the raw material at temperatures from 150 °C to 300 °C at elevated pressures (1.8–2.0 MPa) to dissolve the low reactive silica sand. Therefore, electricity (1.065 tCO_2/t) is the major energy source to produce traditional water glass. In addition, the extraction of raw silica sand also requires energy, for instance, sand dredging, washing and drying.

The CO_2 emission of silica from olivine is only 0.461 tCO_2/t according to a life cycle analysis performed by VTT (EU F7th project, ProMine internal report). It can be calculated from Table 3 that only 0.073 t olivine silica is needed to produce 1 ton of olivine sodium silicate. Silica from olivine dissolves in sodium hydroxide solution at 80 °C and atmospheric pressure in just 2 h, which indicates a significantly lower electricity requirement in the production process for low modulus water glass. In order to calculate the CO_2 emission of precursor for producing 1 ton of silica aerogel, the detailed calculation is shown in Table 11. According to Table 3, the prepared olivine sodium silicate has a silica concentration of 8%, while for commercial water glass, it normally contains a silica concentration of 28 ~ 30%. Therefore, if 1-ton aerogel was produced, it is calculated that 12.5 t olivine sodium silicate or 3.57 t commercial water glass is needed, respectively. The CO_2 footprint in this calculation: Sodium hydroxide pellets (1.915 tCO_2/t), olivine silica (0.46 tCO_2/t), water (0.03 tCO_2/t) and commercial water glass (1.514 tCO_2/t). Therefore, the final calculation

Table 9
Thermal conductivities of reference cellulose/silica aerogel and SCAs.

Groups	SS-CNF1	SS-CNF2	SS-CNF1-M	SS-CNF2-M	NCA1	NCA2	SA
Thermal conductivity (W/m·K)	0.026 ± 0.001	0.023 ± ±0.002	0.030 ± ±0.001	0.029 ± ±0.001	0.036 ± ±0.001	0.038 ± ±0.001	~0.018

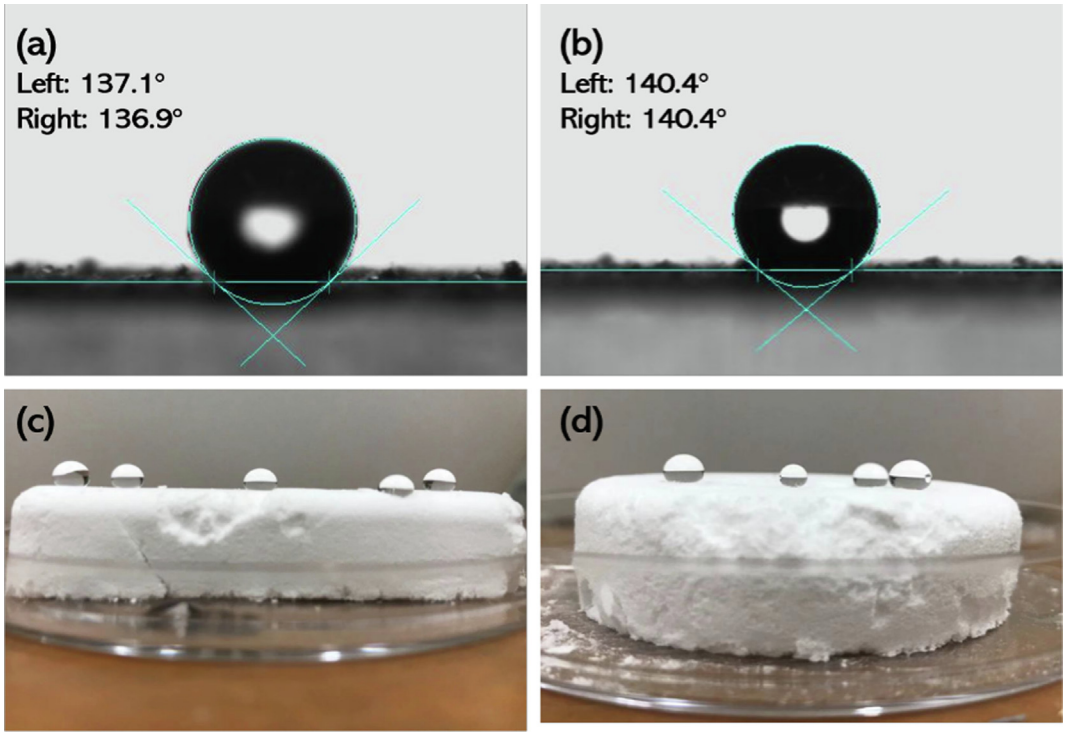

Fig. 10. Water contact angle of SCA: (a) SS-CNF1-M (b) SS-CNF1-M and A few drops of water on the surface of SS-CNF1-M and SS-NFC2-M.

Table 10
LCA of sodium silicate hydrothermally produced in an autoclave [39].

	Emissions from manufacturing	
	Energy (MJ/1000 kg)	Emissions (kg CO_2-e/kg)
Electricity	3118	1.065
Coal	296	0.027
Oil (heavy)	9	0.001
Oil (average/light)	456	0.033
Diesel oil	144	0.010
Gas	1270	0.076
Others	78	0.009
Total	5371	1.222
	Emissions from transport	
	Air emissions (kg/1000 kg)	Emissions (kg CO_2-e/kg)
Carbon dioxide (CO_2)	288.7	0.289
Methane (CH_4)	0.128	0.003
	Total	0.292
	Grand total	1.514

of CO_2 footprint of silicate precursor is the sum of each component used in preparation. Considering aerogel production can be varied due to the solvent exchange and drying method, therefore only the precursor is regarded as a variate and the rest preparation is assumed to be the same. As can be seen, the embedded CO_2 footprint is significantly lower for olivine silica precursor (2.481 tCO_2/t) than commercial water glass (5.517 tCO_2/t).

Moreover, it must be emphasized that the carbon emission of the silica from olivine is calculated without taking the extra heat from the exothermal reaction into account. If this heat can be used, the carbon footprint could be even lowered. Therefore, if only the commercial water glass for aerogel production was replaced to olivine sodium silicate and the rest of the synthesis is the same, the produced aerogel will have a significantly reduced CO_2 footprint and is thus more environmentally friendly.

4. Conclusions

Cellulose aerogel can be function as an ultralightweight material for thermal insulation. However, the limitations of cellulose aerogel including relatively high thermal conductivity and weak mechanical properties have retarded its use in real-world applications. This paper presents a method to prepare green sodium silicate from olivine silica, a low-cost alternative silica source to impregnate silica aerogel within cellulose matrix. The silica-cellulose aerogel (SCA) shows improved compressive strength (95.4 KPa), high surface area (958 m^2/g) and low thermal conductivity (c.a. 23 mW/(m·K)) compared to plain cellulose aerogel. Moreover, it has an ultralow density (0.055 g/cm^3) and high porosity (98%). Based on these results, the following conclusions can be drawn:

- Specific surface area of the SCA reaches c.a. 958 m^2/g for SS-CNF1 and 614 m^2/g for SS-CNF2, compared to pure cellulose

Table 11
Calculation of CO_2 emissions from silicate precursor based on 1 ton of silica aerogel.

Ingredients	NaOH (t)	Olivine silica (t)	Commercial water glass (t)	Water (t)	CO_2 emissions of precursor (tCO_2/t)
Olivine silica-based aerogel	0.88	1.00	N	10.6	2.481
Commercial water glass-based aerogel	N	N	3.5714	N	5.517

N*-Not used.

aerogel with SSA of 200 ~ 300 m^2/g, indicating the sol-gel process of olivine silica derived low modulus silicate can result in higher surface area.
- The compressive strength of SS-CNF1 and hydrophobized SS-CNF1-M increased from 29.8 kPa to 62.8 kPa and 95.4 kPa, respectively, showing the silica-cellulose aerogel has a better mechanical property than plain cellulose aerogel.
- Thermal conductivity of composite silica-cellulose aerogel was significantly lower than pure cellulose aerogel due to the incorporation of fine silica aerogel particles.
- Surface modification by TMCS trimethyl silylation can make SCA composites hydrophobic, with a water contact angle reaching 137.2 ~ 140.4°, which will potentially improve durability and thermal insulating performance of SCAs in the relatively high humidity environment.
- The monolithic silica-cellulose aerogel can be synthesized from low modulus (1.5) silicate sol-gel process. The embedded CO_2 emission of this new aerogel is significantly reduced, reflected by the obviously lower footprint of olivine sodium silicate compared to commercial water glass, namely 2.481 tCO_2/t and 5.517 tCO_2/t, respectively.

CRediT authorship contribution statement

Y.X. Chen: Conceptualization, Methodology, Investigation, Data curation, Formal analysis, Validation, Writing - original draft. **S. Sepahvand:** Writing - review & editing. **F. Gauvin:** Writing - review & editing. **K. Schollbach:** Supervision, Writing - review & editing. **H.J.H Brouwers:** Supervision, Writing - review & editing. **Qingliang Yu:** Conceptualization, Supervision, Writing - review & editing.

Declaration of Competing Interest

The authors declare that they have no known competing financial interests or personal relationships that could have appeared to influence the work reported in this paper.

Acknowledgement

This research was supported by China Scholarship Council (201706950053) and the Department of the Built Environment at Eindhoven University of Technology. Dr. L. Xu from Sappi Nederland Services BV (the Netherlands) is thanked for the CNFs supply.

Appendix A. Supplementary data

Supplementary data to this article can be found online at https://doi.org/10.1016/j.conbuildmat.2021.123289.

References

[1] S.S. Kistler, Coherent expanded aerogels and jellies, Nature. 127 (1931) 741, https://doi.org/10.1038/127741a0.
[2] Z. Yao, W. Li, Microstructure and thermal analysis of APS nano PYSZ coated aluminum alloy piston, J. Alloys Compd. (2020), https://doi.org/10.1016/j.jallcom.2019.152162.
[3] A.C. Pierre, G.M. Pajonk, Chemistry of aerogels and their applications, Chem. Rev. 102 (11) (2002) 4243–4266.
[4] N. Husing, U. Schubert, Aerogel airy materials: chemistry, structure, and properties, Chem. Int. Ed. 37 (1998) 22–45.
[5] J. Fricke, Aerogels-recent progress in production techniques and novel applications, J. Sol-Gel Sci. Technol. 13 (1998) 299.
[6] L.W. Hrubesh, Aerogel applications, J. Non. Cryst. Solids. 225 (1998) 335–342.
[7] C.E. Carraher, General topics: silica aerogel-properties and uses, Polym. News. 30 (2005) 386–388, https://doi.org/10.1080/00323910500402961.
[8] J.L. Gurav, I.-K. Jung, H.-H. Park, E.S. Kang, D.Y. Nadargi, Silica aerogel: synthesis and applications, J. Nanomater. 2010 (2010) 1–11, https://doi.org/10.1155/2010/409310.
[9] S. Liu, T. Yu, N. Hu, R. Liu, X. Liu, High strength cellulose aerogels prepared by spatially confined synthesis of silica in bioscaffolds, Colloids Surfaces A Physicochem. Eng. Asp. 439 (2013) 159–166. 10.1016/j.colsurfa.2012.11.020.
[10] J.T. Korhonen, M. Kettunen, R.H.A. Ras, O. Ikkala, Hydrophobic nanocellulose aerogels as floating, sustainable, reusable, and recyclable oil absorbents, ACS Appl. Mater. Interfaces. 3 (6) (2011) 1813–1816, https://doi.org/10.1021/am200475b.
[11] R. Baetens, B.P. Jelle, A. Gustavsen, Aerogel insulation for building applications: a state-of-the-art review, Energy Build. 43 (4) (2011) 761–769, https://doi.org/10.1016/j.enbuild.2010.12.012.
[12] M. Koebel, A. Rigacci, P. Achard, Aerogel-based thermal superinsulation: an overview, J. Sol-Gel Sci. Technol. 63 (3) (2012) 315–339, https://doi.org/10.1007/s10971-012-2792-9.
[13] L.F. Su, L. Miao, S. Tanemura, G. Xu, Low-cost and fast synthesis of nanoporous silica cryogels for thermal insulation applications, Sci Technol Adv Mater. 13 (2012) 35003, https://doi.org/10.1088/1468-6996/13/3/035003.
[14] R. Ciriminna, A. Fidalgo, V. Pandarus, F. Béland, L.M. Ilharco, M. Pagliaro, The sol-gel route to advanced silica-based materials and recent applications, Chem. Rev. 113 (8) (2013) 6592–6620, https://doi.org/10.1021/cr300399c.
[15] M.A. Aegerter, N. Leventis, M.M. Koebel, Aerogel handbooks, Springer, NewYork, 2011.
[16] M. Fawer, M. Concannon, W. Rieber, Life cycle inventories for the production of sodium silicates, Int. J. Life Cycle Assess. 4 (1999) 207–212, https://doi.org/10.1007/BF02979498.
[17] G. Carlson, D. Lewis, K. McKinley, J. Richardson, T. Tillotson, Aerogel commercialization: technology, markets and costs, J. Non. Cryst. Solids. 186 (1995) 372–379, https://doi.org/10.1016/0022-3093(95)00069-0.
[18] I. Smirnova, P. Gurikov, Aerogel production: current status, research directions, and future opportunities, J. Supercrit. Fluids. (2018), https://doi.org/10.1016/j.supflu.2017.12.037.
[19] Z. Tang, W. Li, V.W.Y. Tam, C. Xue, Advanced progress in recycling municipal and construction solid wastes for manufacturing sustainable construction materials, Resour. Conserv. Recycl. X. (2020), https://doi.org/10.1016/j.rcrx.2020.100036.
[20] A. Lazaro, G. Quercia, H.J.H. Brouwers, J.W. Geus, Synthesis of a green nano-silica material using beneficiated waste dunites and its application in concrete, World J. Nano Sci. Eng. 03 (03) (2013) 41–51, https://doi.org/10.4236/wjnse.2013.33006.
[21] A. Lazaro, M.C. Van De Griend, H.J.H. Brouwers, J.W. Geus, The influence of process conditions and Ostwald ripening on the specific surface area of olivine nano-silica, Microporous Mesoporous Mater. 181 (2013) 254–261, https://doi.org/10.1016/j.micromeso.2013.08.006.
[22] A. Lazaro, N. Vilanova, L.D. Barreto Torres, G. Resoort, I.K. Voets, H.J.H. Brouwers, Synthesis, polymerization, and assembly of nanosilica particles below the isoelectric point, Langmuir. 33 (51) (2017) 14618–14626, https://doi.org/10.1021/acs.langmuir.7b0149810.1021/acs.langmuir.7b01498.s001.
[23] X. Gao, Q.L. Yu, A. Lazaro, H.J.H. Brouwers, Investigation on a green olivine nano-silica source based activator in alkali activated slag-fly ash blends: reaction kinetics, gel structure and carbon footprint, Cem. Concr. Res. 100 (2017) 129–139, https://doi.org/10.1016/j.cemconres.2017.06.007.
[24] Z. Luo, W. Li, Y. Gan, X. He, A. Castel, D. Sheng, Nanoindentation on micromechanical properties and microstructure of geopolymer with nano-SiO2 and nano-TiO2, Cem. Concr. Compos. (2021), https://doi.org/10.1016/j.cemconcomp.2020.103883.
[25] A. Demilecamps, C. Beauger, C. Hildenbrand, A. Rigacci, T. Budtova, Cellulose-silica aerogels, Carbohydr Polym. 122 (2015) 293–300, https://doi.org/10.1016/j.carbpol.2015.01.022.
[26] S. Zhao, Z. Zhang, G. Sèbe, R. Wu, R.V. Rivera Virtudazo, P. Tingaut, M.M. Koebel, Multiscale assembly of superinsulating silica aerogels within silylated nanocellulosic scaffolds: improved mechanical properties promoted by nanoscale chemical compatibilization, Adv. Funct. Mater. 25 (2015) 2326–2334, https://doi.org/10.1002/adfm.201404368.
[27] A. Demilecamps, G. Reichenauer, A. Rigacci, T. Budtova, Cellulose–silica composite aerogels from "one-pot" synthesis, Cellulose. 21 (4) (2014) 2625–2636, https://doi.org/10.1007/s10570-014-0314-3.
[28] H. Sai, L. Xing, J. Xiang, L. Cui, J. Jiao, C. Zhao, Z. Li, F. Li, T. Zhang, Flexible aerogels with interpenetrating network structure of bacterial cellulose-silica composite from sodium silicate precursor via freeze drying process, RSC Adv. 4 (2014) 30453–30461, https://doi.org/10.1039/c4ra02752c.
[29] A. Lazaro, nanosilica production at low temperatures from the dissolution of olivine, Eindhoven University of Technology, 2013.
[30] F. Rafieian, M. Hosseini, M. Jonoobi, Q. Yu, Development of hydrophobic nanocellulose-based aerogel via chemical vapor deposition for oil separation for water treatment, Cellulose. 25 (8) (2018) 4695–4710, https://doi.org/10.1007/s10570-018-1867-3.
[31] S. Sepahvand, M. Jonoobi, A. Ashori, F. Gauvin, H.J.H. Brouwers, K. Oksman, Q. Yu, A promising process to modify cellulose nanofibers for carbon dioxide (CO2) adsorption, Carbohydr. Polym. (2020), https://doi.org/10.1016/j.carbpol.2019.115571.
[32] A. Demilecamps, G. Reichenauer, A. Rigacci, T. Budtova, Cellulose-silica composite aerogels from "one-pot" synthesis, Cellulose. 21 (4) (2014) 2625–2636, https://doi.org/10.1007/s10570-014-0314-3.
[33] H. Maleki, L. Durães, A. Portugal, An overview on silica aerogels synthesis and different mechanical reinforcing strategies, J. Non. Cryst. Solids. 385 (2014) 55–74, https://doi.org/10.1016/j.jnoncrysol.2013.10.017.

[34] J.C.H. Wong, H. Kaymak, S. Brunner, M.M. Koebel, Mechanical properties of monolithic silica aerogels made from polyethoxydisiloxanes, Microporous Mesoporous Mater. 183 (2014) 23–29, https://doi.org/10.1016/j.micromeso.2013.08.029.
[35] S. He, X. Chen, Flexible silica aerogel based on methyltrimethoxysilane with improved mechanical property, J. Non. Cryst. Solids. 463 (2017) 6–11, https://doi.org/10.1016/j.jnoncrysol.2017.02.014.
[36] S. Cui, Y.u. Liu, M.-H. Fan, A.T. Cooper, B.-L. Lin, X.-Y. Liu, G.-F. Han, X.-D. Shen, Temperature dependent microstructure of MTES modified hydrophobic silica aerogels, Mater. Lett. 65 (4) (2011) 606–609, https://doi.org/10.1016/j.matlet.2010.11.026.
[37] G. Hayase, K. Kanamori, K. Kazuki, T. Hanada, synthesis of new flexible aerogels from MTMS/DMDMS via ambient pressure drying, IOP Conf. Ser. Mater. Sci. Eng. 18 (2011) 32013, https://doi.org/10.1088/1757-899x/18/3/032013.
[38] L.K. Turner, F.G. Collins, Carbon dioxide equivalent (CO2-e) emissions: a comparison between geopolymer and OPC cement concrete, Constr. Build. Mater. 43 (2013) 125–130, https://doi.org/10.1016/j.conbuildmat.2013.01.023.
[39] Life cycle inventories for the production of sodium silicates, Int J LCA. 4 (1999) 207.